Please cite this article in press as: Alkuraya et al., Human Mutations in *NDE1* Cause Extreme Microcephaly with Lissencephaly, The American Journal of Human Genetics (2011), doi:10.1016/j.ajhg.2011.04.003

ARTICLE

Human Mutations in *NDE1* Cause Extreme Microcephaly with Lissencephaly

Fowzan S. Alkuraya,[1,8,9,11] Xuyu Cai,[2,3,11] Carina Emery,[4] Ganeshwaran H. Mochida,[2,5,6] Mohammed S. Al-Dosari,[1,10] Jillian M. Felie,[2] R. Sean Hill,[2] Brenda J. Barry,[2] Jennifer N. Partlow,[2] Generoso G. Gascon,[7] Amal Kentab,[9] Mohammad Jan,[7] Ranad Shaheen,[1] Yuanyi Feng,[4,*] and Christopher A. Walsh[2,3,5,*]

Genes disrupted in human microcephaly (meaning "small brain") define key regulators of neural progenitor proliferation and cell-fate specification. In comparison, genes mutated in human lissencephaly (*lissos* means *smooth* and *cephalos* means *brain*) highlight critical regulators of neuronal migration. Here, we report two families with extreme microcephaly and grossly simplified cortical gyral structure, a condition referred to as microlissencephaly, and show that they carry homozygous frameshift mutations in *NDE1*, which encodes a multidomain protein that localizes to the centrosome and mitotic spindle poles. Both human mutations in *NDE1* truncate the C-terminal NDE1domains, which are essential for interactions with cytoplasmic dynein and thus for regulation of cytoskeletal dynamics in mitosis and for cell-cycle-dependent phosphorylation of NDE1 by Cdk1. We show that the patient NDE1 proteins are unstable, cannot bind cytoplasmic dynein, and do not localize properly to the centrosome. Additionally, we show that CDK1 phosphorylation at T246, which is within the C-terminal region disrupted by the mutations, is required for cell-cycle progression from the G2 to the M phase. The role of NDE1 in cell-cycle progression probably contributes to the profound neuronal proliferation defects evident in *Nde1*-null mice and patients with *NDE1* mutations, demonstrating the essential role of *NDE1* in human cerebral cortical neurogenesis.

Introduction

The exquisitely organized formation of cerebral cortical neurons from the cortical neuroepithelium has provided an important system for studying the control of cell proliferation and cell fate. Cortical progenitors, forming a pseudostratified epithelium with nuclei in the ventricular germinal zone, have the capacity to undergo symmetrical cell divisions to form two dividing daughter cells or asymmetrical cell divisions to generate one dividing daughter and postmitotic neurons that populate the developing cortex. After exiting the cell cycle, postmitotic neurons migrate away from the ventricular zone to the incipient cerebral cortical layers to establish the highly organized cortical architecture. Human autosomal-recessive primary microcephaly (MCPH [MIM 251200]), or microcephaly vera, manifests as small but architecturally fairly normal brains. Multiple human genes mutated in MCPH encode proteins that localize to the centrosome and/or mitotic spindle poles.[1] Many of them have also been implicated in regulating progenitor cell-cycle progression and in determining whether progenitors will continue proliferating or differentiate into postmitotic neurons.[1] In contrast to microcephaly, human lissencephaly manifests as a simplified cortical gyration pattern that reflects abnormal histological organization of the cortical layers but normal brain volume and thus most often reflects disruption of neuronal migration.[2] Identified genetic causes of lissencephaly include mutations in *LIS1* (MIM 601545),[3] *DCX* (MIM 300121),[4] *RELN* (MIM 600514),[5] and *TUBA1A* (MIM 602519).[6] Recently, mutations in *WDR62* [MIM 613583] have been associated with microcephaly and with a variety of architectural defects of the cortex,[7–9] suggesting additional overlap in the genes that regulate proliferation and migration. However, there have long been rare cases in which a reduced brain size typical of microcephaly is also associated with simplification of cerebral cortical gyration that falls within the spectrum of lissencephaly. These two findings together have been referred to as "microlissencephaly[10,11]," but the genetic and mechanistic causes of microlissencephaly are unknown.

Nuclear distribution E (NudE) was originally identified in *Aspergillus nidulans* as an essential regulator of a common nuclear migration pathway, which also involves *NudC* (*DYNC1H1* [MIM 600112]) and *NudF* (*LIS1*).[12] The mammalian orthologs of *NudE* include *NDE1* (MIM 609449) and *NDE1-Like 1* (*NDEL1* [MIM 607538]). *Nde1* is highly expressed in cortical neural progenitors and encodes a protein that localizes to the centrosome and mitotic spindle poles. This protein is also known to

[1]Department of Genetics, King Faisal Specialist Hospital and Research Center, Riyadh 11211, Saudi Arabia; [2]Division of Genetics, Howard Hughes Medical Institute, and Manton Center for Orphan Disease Research, Children's Hospital Boston, Boston, MA 02215, USA; [3]Program in Biomedical and Biological Sciences, Harvard Medical School, Boston, MA 02215, USA; [4]Department of Neurology and Center for Genetic Medicine, Northwestern University Feinberg School of Medicine, Chicago, IL 60611, USA; [5]Departments of Pediatrics and Neurology, Harvard Medical School, Boston, MA 02215, USA; [6]Pediatric Neurology Unit, Department of Neurology, Massachusetts General Hospital, Boston, MA 02114, USA; [7]Department of Neurology, King Faisal Hospital and Research Centre, Jeddah 11211, Saudi Arabia; [8]Department of Anatomy and Cell Biology, College of Medicine, Alfaisal University, Riyadh 11533, Saudi Arabia; [9]Department of Pediatrics, King Khalid University Hospital and College of Medicine, King Saud University, Riyadh 11472, Saudi Arabia; [10]Department of Pharmacognosy, College of Pharmacy, King Saud University, Riyadh 11451, Saudi Arabia
[11]These authors contributed equally to this work
*Correspondence: yuanyi-feng@northwestern.edu (Y.F.), christopher.walsh@childrens.harvard.edu (C.A.W.)
DOI 10.1016/j.ajhg.2011.04.003.

physically interact with the cytoplasmic dynein complex and Lis1.[13–15] The dynein-Lis1-Nde1 complex has an essential role in the cytoskeleton dynamics of a wide range of cellular processes, including mitosis, nuclei positioning, and cell migration.[2,16] Loss of *Nde1* in mouse models causes profound defects in cerebral corticogenesis but only modest defects in neuronal migration.[14] *Nde1*-null cortical progenitors showed defects in centrosome duplication and mitotic-spindle assembly. These mitotic defects resulted in severe mitotic arrest or delay, spindle misorientation, and mispositioning of the mitotic chromosomes and were thought to account for the premature depletion of progenitor cells in *Nde1*-null brains through impaired cell-cycle progression and for premature cell-cycle exit by progenitors to form neurons.[14]

In this study, we demonstrate that *NDE1* mutations cause a severe microlissencephaly syndrome resembling that described initially by Norman and Roberts.[10,11] The identified frameshift mutations result in truncation of the C-terminal domains and disruption of several key functions of NDE1. Additionally, we show that Nde1 is phosphorylated by Cdk1 and that CDK1 phosphorylation at T246, within the C-terminal region that is disrupted by both mutations, is required for cells to progress through the G2/M phase of mitosis.

Subjects, Material, and Methods

Human Studies

The human studies protocols were reviewed and approved by the institutional review board of the Children's Hospital Boston and the King Faisal Specialist Hospital and Research Centers at Riyadh and Jeddah and performed in accordance with the ethical standards. Proper informed consent was obtained. Standard protocols were used for blood draw and DNA extractions.

Genome-wide Linkage Analysis

We genotyped family 1 by using the Affy 250K *Sty*I SNP Chip as per the manufacturer's protocol and family 2 by using the Illumina660W-Quad Chip at the W.M. Keck Foundation Biotechnology Resource Laboratory at Yale University. We calculated single and multipoint LOD scores by using Allegro and assuming a recessive mode of disease inheritance, full penetrance, and a disease-allele frequency of 0.0001.

Nucleotide numbers are in reference to cDNA (RefSeq NM_017668.2, where A of the ATG translational start site is designated as +1) coordinates, and amino acid numbers are in reference to protein (RefSeq NP_001137451.1) coordinates, per HGVS guidelines.

Sanger Sequencing

We amplified *NDE1* coding exons as well as flanking intronic sequences by PCR, and then either bidirectionally sequenced them by using ABI 3730XL DNA Analyzer or submitted them to Polymorphic DNA Technologies for Sanger capillary electrophoresis. See Table S1 for PCR primer sequences and conditions. Sequencing of more than 200 neurologically normal control samples and 96 unaffected individuals from Saudi Arabian families with unrelated disorders failed to identify either mutant variant.

Cell Culture, Transfection, Cell Synchronization, and Flow Cytometry

293T cells were cultured in Dulbecco's Modified Earle Medium (DMEM) containing 10% fetal bovine serum (FBS). Mouse embryonic fibroblasts (MEFs) were isolated from E13.5 *Nde1*$^{-/-}$ mice and their littermates and were cultured in DMEM with 10% FBS for no more than two passages. We transformed human lymphoblasts from normal and *NDE1*$^{-/-}$ individuals and from heterozygous *NDE1*$^{-/+}$ parents by using Epstein-Barr virus and cultured them in RPMI medium supplemented with 15% fetal calf serum (FCS). For FLAG-NDE1 overexpression, we transfected 293T cells with specified plasmids (empty FLAG-containing vector, FLAG-NDE1-WT, FLAG-NDE1–p.Pro229TrpfsX85, and FLAG-NDE1-p.Leu245ProfsX70) by using *Fugene6* (Roche). For Cdk1 and MAPK knockdown, we cotransfected *Silencer* Select Pre-Designed and Validated siRNAs (Applied Biosystems) designed against Cdk1, MAPK1, and MAPK3 at12 nM with Nde1-WT or Nde1-T246A plasmids into 293T cells for 48 hr by using lipofectamine (Invitrogen) as indicated. For cells with enriched G0 and G2/M populations, 293T cells were starved of serum in DMEM for 48 hr (G0) and recovered in 10% serum for 3 hr; 0.1 μM nocodazole was added for 24 hr so that cells would arrest at G2/M. The flow-cytometry study was performed as previously described;[14] mitotic cells were labeled with phospho-histone H3 antibody, and about 60,000 cells were analyzed for each sample.

To measure the mitotic index, we fixed MEFs at passage 1 with cold methanol, and we identified cells in G2/M by the MPM-2 antibody immunostaining. We counted approximately 1500 cells from 10 randomly selected fields, and we identified percentages of MPM-2-positive versus total cells by using Hoechst 33342 staining. We performed the statistical analysis by using the chi-square test of homogeneity for two independent samples.

Immunoblotting and Immunoprecipitation

We prepared cell lysates by using either lysis buffer (for immunoprecipitation) containing 50 mM Tris-HCl (pH 7.4), 150 mM NaCl, 0.4% NP-40, 1 mM NaF, 10 mM b-glycero-phosphate, 10 nM calyculin A, 1 mM Na3VO4, 1 mM PMSF, and a protease inhibitor cocktail mix (Roche) or (for direct immunoblotting) RIPA buffer (50 mM Tris-HCl 7.4, 150 mM NaCl, 1% NP-40, 0.5% sodium deoxycholate, and 0.1% SDS) containing a protease inhibitor cocktail mix (Roche). We normalized protein concentrations by using the bicinchoninic acid assay (Thermo Scientific). For immunoprecipitation, cell lysates were incubated with anti-FLAG M2 affinity gel (Sigma) for 2 hr at 4°C and then washed three times with the same lysis buffer. Protein samples were then eluted with 3XFLAG peptides (150 ng/μl) for 1 hr at 4°C. For immunoblotting, cell lysates or immunoprecipitation elution were boiled in LDS sample buffer (Invitrogen) and then electrophoresed on 4%–12% Bis-Tris or 7% Tris-Acetate SDS-PAGE (Invitrogen) and transfered onto a PVDF membrane (Millipore). We blocked membranes for 30 min in TBST that contained 5% nonfat milk or Odyssey Blocking Buffer (LICOR Biosciences) at room temperature, incubated them with primary antibodies according to the antibody manufacturer's instructions, and then incubated them with HRP-conjugated secondary antibodies (Cell Signaling Technology) or fluorescent-dye-conjugated secondary antibodies (LICOR Biosciences). Immunosignals were detected by

SuperSignal West Pico Chemiluminescent (Pierce) or the Odyssey Infrared Imaging System (LICOR Biosciences).

To create a phospho-specific antiserum against T246 of NDE1, we coupled a synthetic peptide corresponding to amino acids R234–T246 of Nde1 that includes a phosphorylated T246 residue (p-Nde1T246) to KLH and used it to immunize rabbits via standard procedures provided by Covance. The resulting antisera were purified against Affi-Gel 10 and 15 columns (Biorad) to which the p-Nde1T246 peptide was coupled. The affinity-purified p-Nde1T246 peptide antisera were further purified through a column coupled with unphosphorylated Nde1T246 peptide to deplete immunoreactivities against unphosphorylated proteins. The rabbit antibody against total Nde1 was used as previously described.[14] In addition, the following antibodies were purchased and used according to the manufacturer's instructions: mouse FLAG (M2) antibody and anti-FLAG beads (Sigma), rabbit anti-DYKDDDDK (FLAG) (Cell Signaling Technology), rabbit anti-LIS1 (Bethyl Laboratory), mouse monoclonal anti-dynein intermediate chain (clone 74.1) (Millipore), rabbit anti-dynein heavy chain (Santa Cruz Biotechnology), mouse monoclonal anti-Cdk1 (Millipore), rabbit anti-p42/44 MAP kinase (Cell Signaling Technology), and mouse anti-MPM-2 (Upstate). Immunohistochemistry and immunocytochemistry protocols are described in detail elsewhere.[14]

For the FLAG-NDE1 construct, *NDE1* cDNA (RefSeq NM_017668.2, starting from ATG) was amplified by PCR and subcloned into the p3XFLAG-CMV-10 vector (Sigma); the two mutant constructs were generated by site-directed mutagenesis so that 684_685AC (c.684_685del; p.Pro229TrpfsX85) was deleted or 733C (c.733dup; p.Leu245ProfsX70) was duplicated, respectively. Nde1-T246A construct was generated by site-directed mutagenesis on Nde1-WT cDNA construct as described previously.[14]

In Vitro Cdk1/Cdc2 Kinase Assay

Myc-tagged Nde1 and Nde1 point mutants were expressed in 293T cells and immunoprecipitated with the 9E10 Myc monoclonal antibody. Recombinant cyclin B1 and Cdk1/Cdc2 were purchased from New England Biolabs, and the kinase assay was performed with the reaction buffer provided by the manufacturer. After the immunocomplexes were washed and equilibrated to the kinase reaction buffer, they were incubated with 0.1 unit of Cdk1/Cdc2 kinase and 50 μM [γ−32P] ATP (specific activity of 100 μCi/μmol) at room temperature for 10 min. The reaction products were analyzed by 10% SDS PAGE followed by autoradiography.

Results

Clinical Characterization of Microlissencephaly

Ongoing efforts to characterize the genetic bases of microcephaly by a large collaborative effort known as the Microcephaly Collaborative (Table S2, available online) have identified two families whose children share remarkably severe microcephaly (head circumferences more than 11 and 13 standard deviations [SD] below the mean for age), abnormal cortical gyration, short length (more than 2 and 4 SD below the mean for age), microsomia (weight more than 2 and 5 SD below the mean for age) and a prominent broad nasal bridge (Figure 1); both families have been approved by the institutional review board.

Family 1 originates from eastern Saudi Arabia. The parents are healthy and are reported to be first cousins. They have two daughters affected by extreme microcephaly (Figure 1A). The first affected daughter (08DG00535; family1, IV-1 in Figure 1A) was first evaluated at the age of 33 months, at which time her head circumference was 34.4 cm, length was 81.4 cm, and weight was 8.6 kg (8.9, 3, and 3.8 SD below the mean, respectively). Physical examination at that time was notable for marked hypertonia and global developmental delay. Magnetic resonance imaging (MRI) scans revealed severe microcephaly with a proportionate reduction in the size of most other brain structures, including the cerebellum and brain stem, associated with agenesis of the corpus callosum. The gyral folding of the cerebral cortex was extremely simplified; there were almost no detectable sulci other than the Sylvian fissure. At the age of 7 years, she displayed extreme microcephaly (the head circumference of 35 cm was 13.4 SD below the mean) and evidence of retarded growth; she had a length of 105 cm and weight of 10 kg (3.1 and 4.7 SD below the mean, respectively). She remained seizure-free but was only able to roll over, and her social and cognitive development was limited to spontaneous smiling. The second affected daughter (08DG00536; family 1, IV-2 in Figure 1A) was first evaluated at birth, at which time her length and weight were normal, head circumference was 26.5 cm (5.6 SD below the mean), and anterior fontanelle was almost closed. Her neurological course was static and characterized by marked hypertonia; she gained virtually no milestones beyond spontaneous smiling and rolling over by the age of 5.5 years but developed no seizures. At that time her head circumference was 34 cm, length was 85 cm, and weight was 8.9 kg (12.7, 5.5, and 4.8 SD below the mean, respectively). Laboratory investigations, including plasma acylcarnitines, carnitine, amino acids, urine organic acids, ammonia, lactic acid, and high-resolution karyotype, were all normal. MRI scans showed microcephaly, severe simplification of the gyral pattern (lissencephaly), agenesis of the corpus callosum, and colpocephaly (enlargement of the posterior lateral ventricles, often associated with corpus callosum defects), features that have been described in microlissencephaly (Figures 1B–1G; see Movies S1–S6).

Family 2 originates from western Saudi Arabia. The parents are healthy and are reported to be first cousins. They have a daughter and son with extreme microcephaly and two healthy sons and had three additional pregnancies that resulted in spontaneous abortions (Figure 1A). The affected daughter was reported to have microcephaly without seizures, but no additional information was available (family 2, II-4 in Figure 1A). The affected son (MC-14901; family 2, II-7 in Figure 1A) displayed microcephaly and dysmorphic features at birth, but growth parameters were not available. A head CT at that time revealed small brain size. Seizures began at two months of age and were described as starting on the left side and progressing to full-body convulsions with up-rolling of the eyes. He was first evaluated at 9 months of age, at which time he could not roll or control his head, and

Please cite this article in press as: Alkuraya et al., Human Mutations in *NDE1* Cause Extreme Microcephaly with Lissencephaly, The American Journal of Human Genetics (2011), doi:10.1016/j.ajhg.2011.04.003

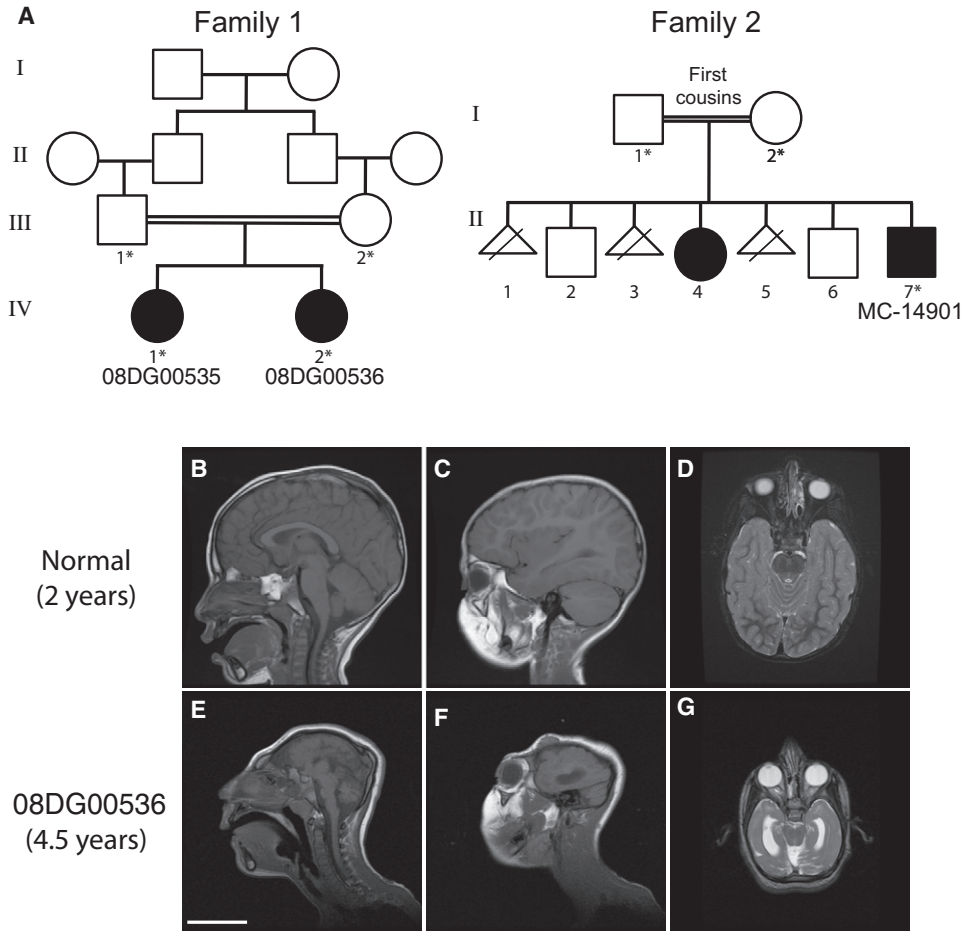

Figure 1. Pedigrees and Radiographic Features of the Two Consanguineous Families with Microlissencephaly
(A) Both families are from Saudi Arabia. Parents of family 1 are first cousins and have two affected female children (08DG00535, IV-1 and 08DG00536, IV-2). Whole-blood DNA from both parents and both affected children was obtained and analyzed (indicated by an asterisk). Parents of family 2 are first cousins who had seven reported pregnancies, producing one affected male (MC-14901, II-7), one affected female (II-4) (not available for analysis), two unaffected males, and three pregnancies that resulted in fetal demise. Whole-blood DNA from both parents and the affected male (MC-14901, II-7) was obtained and analyzed (indicated by an asterisk).
(B–G) Representative MRI images of 08DG00536 (IV-2) from family 1 at 4.5 years of age, demonstrating the drastic reduction in brain size (E–G), agenesis of the corpus callosum, and abnormal gyral pattern compared to that seen in a normal 2-year-old child (B-D). Sagittal T1 (B, C, E, and F) and axial T2 (D and G) sections are shown. The scale bar represents 5 cm. Additional images are available as Movies S1–S6.

a neurologic exam revealed increased reflexes, decreased tone, normal power, and positive Babinski signs. MRI scans at 11 months of age showed a marked decrease in the size of both cerebral hemispheres, a large midline fluid-filled structure, dilatation of the right lateral ventricle, a small cerebellum, and agenesis of the corpus callosum. The thalami were not fused, and a midline falx was noted. Laboratory investigations revealed a normal karyotype (46, XY), an unremarkable acylcarnitine profile, and normal amino acid analysis by tandem mass spectrometry. An evaluation at 3.5 years of age recorded his head circumference as 32 cm (11.1 SD below the mean), length as 88 cm (2.8 SD below the mean), and weight as 13 kg (6th percentile).

Identification of Homozygous *NDE1* Mutations

All patients were born to consanguineous marriages, suggesting autosomal inheritance and allowing homozygosity mapping, which identified only one common homozygous region larger than 1Mb—at chromosome 16p13.11—shared by all three affected children (DNA from the second affected child in family 2 was unavailable). The maximal LOD scores of the two pedigrees at the homozygous region are 1.8 and 1.2, respectively. The homozygous locus is 4.6 Mb in size and contains approximately 35 annotated genes, including *NDE1* (Figure 2A). *NDE1* was selected as the top candidate given that the *Nde1* mutations strongly affected neural progenitor proliferation and that defects of both proliferation and neuronal migration were observed in mice deficient for both *Nde1* and *Lis1*.[14,17,18] Direct sequencing of *NDE1* revealed frameshift mutations in both families (Figures 2B and 2C). Family 1 showed a c.684_685del mutation in exon 6 that creates a translational frameshift at codon 229 of the normal 335 amino acid protein sequence (p.Pro229TrpfsX85) and predicts a protein that consists of 312 amino acids, terminating after

the addition of 84 abnormal amino acids (Figures 2B and 2C). Exon 7 of family 2 showed a c.733dup mutation that creates a frameshift mutation at codon 245 (into the same abnormal reading frame as the mutation in family 1). This frameshift is predicted to result in a protein that is truncated after the addition of 69 abnormal amino acids (p.Leu245ProfsX70). Both mutations were homozygous in affected individuals; segregated perfectly with disease in each family; were absent from more than 200 normal individuals, including 96 Saudi Arabian controls; and were not seen in the 1000 Genomes Project, all of which strongly suggests that they are bona fide mutations. This conclusion was further supported by identification of additional *NDE1* alleles in patients sharing similar clinical features by Bakircioglu et al.[19] in this issue.

Characterization of the Mutant NDE1 Proteins

On the basis of data from *NDE1* and its paralog, *NDEL1*, it appears that the truncated NDE1 proteins, if stable, would lack critical protein domains (Figure 2B). The C terminus of NDE1 includes a domain required for interaction with CENP-F, which directs NDE1 to kinetochores,[20] and another domain that regulates binding to the cytoplasmic dynein complex[21,22] and to Su48,[23] which was recently found to regulate centrosomal localization of NDE1. Although RT-PCR with patient lymphoblasts from family 1 suggested an equal abundance of *NDE1* transcripts between patients and controls (data not shown), immunoblot analysis of patient lymphoblasts showed no detectable NDE1 protein in the two affected patients (family 1, IV-I and IV-II) carrying the p.Pro229TrpfsX85 mutation (Figure 3A), whereas the heterozygous parents showed an ~50% reduction in protein levels. These data suggest that the frameshift mutation caused instability of the protein and subsequent degradation. Thus, the severe reduction in brain volume in these patients is far more severe than the dramatic *ASPM*-associated microcephaly[24–26] and appears to be associated with loss of the NDE1 protein, although some mutant protein in some tissues cannot be ruled out.

In order to further study the functional role of the C terminus of NDE1, we engineered cDNAs corresponding to the p.Pro229TrpfsX85 and p.Leu245ProfsX70 alleles and fused them with FLAG tag (Figure 2B). Despite the possible protein instability of endogenous mutant proteins, overexpression allowed recovery of enough protein so that the effects of the two mutations on NDE1 binding to LIS1 and to dynein could be studied. Wild-type FLAG-NDE1 can be easily coimmunoprecipitated with the dynein complex (Figure 3B), and both frameshift mutants completely abolished dynein binding (Figure 3C). NDE1 also binds LIS1 but through the coiled-coil domain at the amino terminus of NDE1,[13,27] and LIS1 binding was normal or even enhanced (Figure 3C) in the FLAG-tagged mutant proteins. Because during neurogenesis the cytoplasmic dynein complex has profound roles, including mitotic spindle organization, interkinetic nuclear migration, and neuronal migration, the loss of an important dynein regulator could impact multiple aspects of neurogenesis.

Both mutations are also predicted to abolish the centrosomal localization domain located at the C terminus of NDE1 (Figure 2B). To examine the effects of mutations on NDE1 subcellular localization, we transfected GFP-tagged wild-type or p.Leu245ProfsX70 mutant NDE1 in 293T cells. Wild-type GFP-NDE1 localized to the centrosome, consistent with previous findings (Figure 3D), whereas mutant GFP-NDE1-p.Leu245ProfsX70 failed to target the centrosome but either presented as noncentrosomal aggregates or presented diffusely in the cytoplasm. (Figures 3E and 3F). Similar results were reported by Bakircioglu et al.[19] after analyzing the p.Pro229TrpfsX85 allele. Therefore, both *NDE1* mutations disrupt at least two key functions of NDE1, suggesting that the developmental defects seen in the patients are likely caused by the loss of *NDE1* function.

Phosphorylation by Cdk1 at Nde1 T246 Regulates G2/M Transition

The p.Pro229TrpfsX85 and p.Leu245ProfsX70 alleles also eliminate key potential phosphorylation sites in the C terminus of NDE1. We previously reported that NDE1 redistributes when cells enter mitosis.[14] In addition, Nde1 and its paralog, Ndel1, have been reported as mitotic phospho-proteins.[28] Phosphorylation of NDEL1 by the mitotic kinases Cdk1/Cdc2 and Aurora-A are involved in cell-cycle-dependent events such as centrosome maturation, G2/M transition, and microtubule remodeling during mitosis.[2,29,30] We confirmed that NDE1 and Nde1 are also regulated by mitotic phosphorylation; NDE1 extracted from mitotically arrested cells (G2/M) often appeared in slowly migrating forms on immunoblots compared to the NDE1 from cells arrested at G0 in serum-free media; this suggests increased phosphorylation (Figure 4A). Scansite analysis[31] identified putative Cdk1/Cdc2 phosphorylation sites on NDE1 that are conserved in NDEL1[30,32,33] (Figure 4B), whereas threonine 246 of NDE1 and Nde1 is predicted as the most favorable Cdk1 target at high stringency by Scansite, is the most conserved site across species (Figure 4B), and is the only site removed by both mutations. To investigate the potential regulation of Nde1 by mitotic phosphorylation, we generated an antiserum that specifically recognizes phospho-T246 of Nde1 (p-Nde1T246). The slowly migrating Nde1 band seen in G2/M-arrested cells is specifically recognized by this phospho-T246 antiserum, confirming that NDE1 is phosphorylated at T246 at G2/M. Immunofluorescence studies with the same antiserum showed that it recognizes cells that appear to be at G2/M (Figure 4C) and highlighted metaphase neocortical apical progenitors along the surface of lateral ventricles in mouse developing brains (Figure 4D).

To test whether T246 of Nde1 is a Cdk1/Cdc2 target, we showed that knockdown of Cdk1 specifically abolished the

Please cite this article in press as: Alkuraya et al., Human Mutations in *NDE1* Cause Extreme Microcephaly with Lissencephaly, The American Journal of Human Genetics (2011), doi:10.1016/j.ajhg.2011.04.003

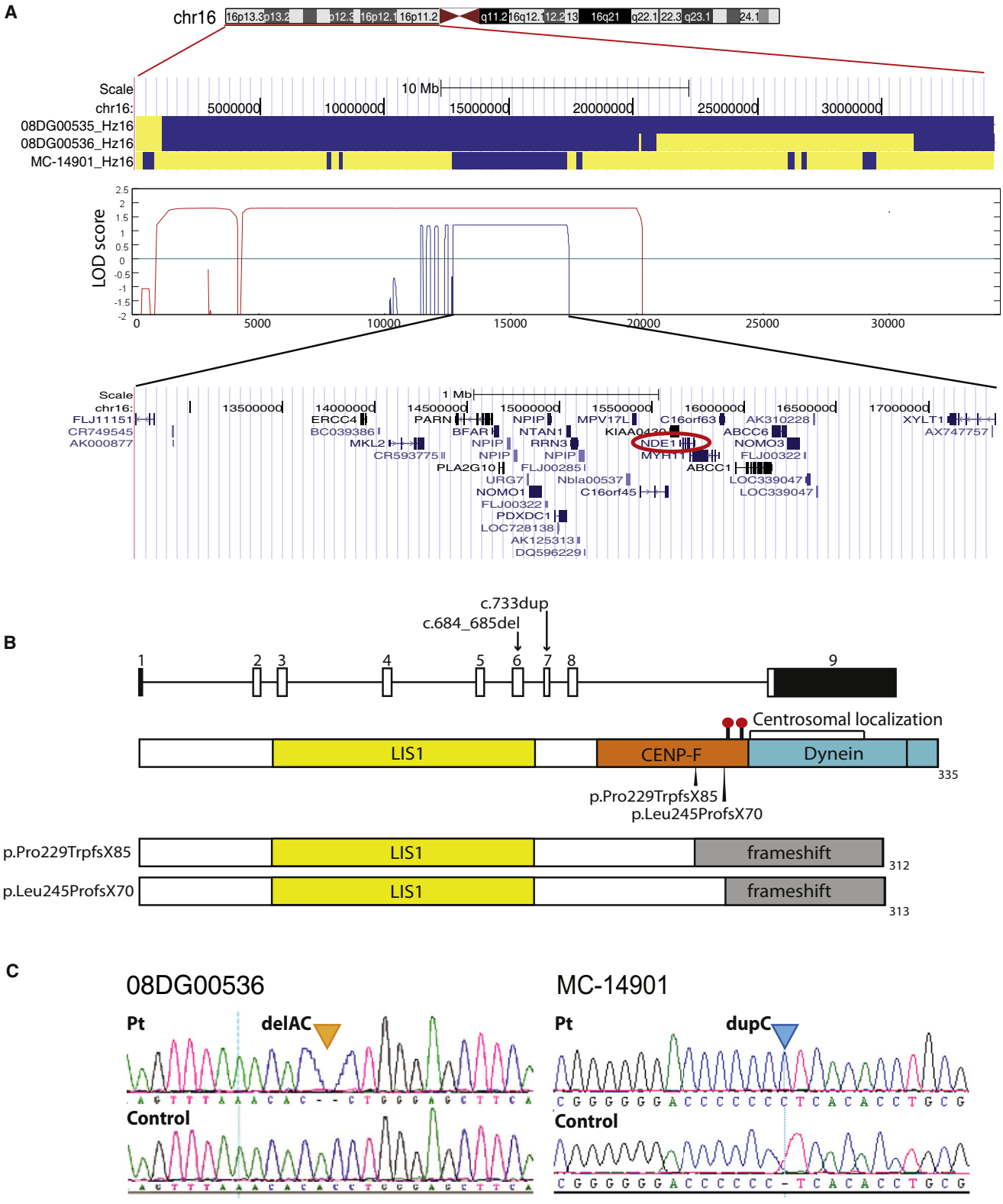

Figure 2. Two *NDE1* Mutations Identified within an Overlapping Region of Homozygosity in Both Pedigrees on Chromosome 16

(A) Homozygosity analysis of both pedigrees identified a 4.6 Mb region on chromosome 16 that is homozygous in all three affected children. All homozygous SNPs are represented as blue, and heterozygous SNPs are represented as yellow. The maximal LOD scores of the two pedigrees at the homozygous region are 1.8 and 1.2, respectively. The shared region of homozygosity contains approximately 35 annotated genes, including *NDE1*.

(B) Human *NDE1* consists of nine exons (eight coding exons), which encode a protein with 335 amino acids harboring multiple protein-interaction domains. Two frameshift mutations were indentified in exons 6 and 7, respectively; both are predicted to disrupt the CENP-F, dynein interaction domain, centrosomal localization domain, and at least two conserved phosphorylation residues implicated in

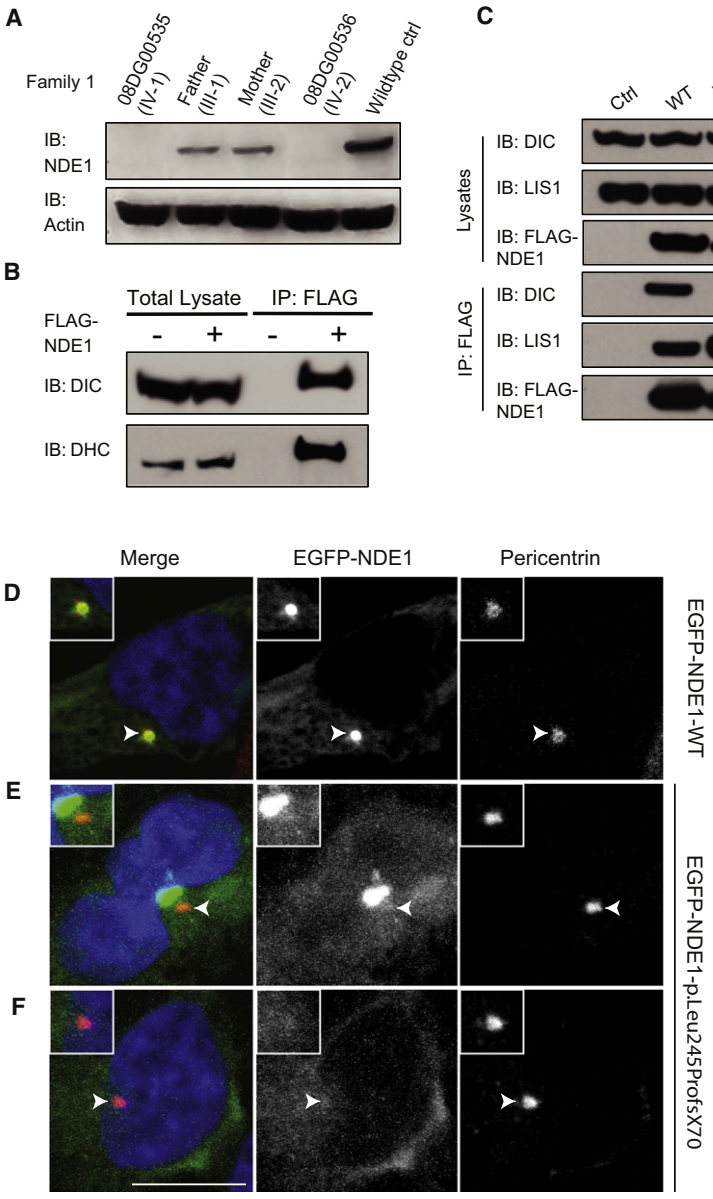

Figure 3. The Mutant NDE1 Proteins Are Unstable and Lack Critical Functions

(A) NDE1 protein was undetectable in the whole-cell lysates collected from lymphoblasts of both patients (IV-1 and IV-2 in Figure 1A) in family 1 harboring the c.684_685del mutation. The protein levels of NDE1 from the parents (III-1 and III-2 in Figure 1A) were reduced by roughly 50% in comparison to the wild-type control; this is consistent with their known heterozygous carrier status. Immunoblotting (IB) was performed with an antibody against NDE1 and actin as a loading control.

(B) Wild-type FLAG-NDE1 interacts with the dynein complex. Immunoprecipitation was performed with anti-FLAG M2 beads. Cells transfected with empty 3XFLAG-CMV vector were labeled as "−" and used as the negative control; cells transfected with wild-type FLAG-NDE1 vector were labeled as "+." The following abbreviations are used: DIC, dynein intermediate chain 74.1; DHC, dynein heavy chain.

(C) The interaction with the dynein complex was abolished in both mutant NDE1 proteins, which confirms the disruption of the dynein-binding domain by both mutant alleles. However, the interaction with LIS1 was preserved or even slightly enhanced in both mutant proteins.

(D–F) The centrosomal localization of NDE1 was abolished in the mutants. (D) Wild-type EGFP-NDE1-WT was transfected into 293T cells and localized to the centrosome. (E and F) Mutant EGFP-NDE1-p.Leu245ProfsX70 was transfected into 293T cells and did not localize to the centrosome. It either formed noncentrosomal aggregates (E) or localized diffusely in the cytoplasm. (F) Centrosomes labeled by pericentrin are indicated by the arrowheads and magnified in the upper left insets. The scale bar indicates 10 μm.

p-Nde1T246 immunosignal and left the total Nde1 protein level unchanged (Figure 4E). Although the flanking sequence of Nde1 T246 also matches a preferred Erk1/2 phosphorylation site, PXTP, knockdown of Erk1 (MAPK3) or Erk2 (MAPK1) showed little effect on p-NdelT246 levels (Figure 4E), suggesting that NDE1 T246 is not a preferred target of MAPK1 or MAPK3 in vivo. Furthermore, we showed that recombinant Cdk1 was able to phosphorylate Myc-Nde1 that had been immunoprecipitated in vitro (Figure S1). Interestingly, mutating T215, T246, or both into phosphorylation-deficient residues (p.T215A, p.T246A, and p.T215/T246A, respectively) reduced but did not abolish the ^{32}P signal; this suggests that additional sites on Nde1 are also phosphorylated by Cdk1 in vitro. Finally, to test whether the phosphorylation of T246 is functionally important, we overexpressed the Nde1-T246A mutant and found that cells expressing this T246 phosphorylation-deficient mutant arrest at the G2 phase with increased 4N DNA content but with reduced pH3+ staining, a marker that identifies the mitotic population (Figure 4F). These data suggest that phosphorylation of T246 is essential for the G2/M transition and is consistent

mitotic progression (T246 and S250) at the C terminus. The black bars show noncoding exons; open bars show coding exons. The red dots indicate potential phosphorylation sites.

(C) Representative Sanger sequencing traces indicating the two base-pair deletions identified in patient 08DG00536 (family 1, IV-2 in Figure 1A) and the one base-pair duplicated identified in patient MC-14901 (family 2, II-7 in Figure 1A).

Please cite this article in press as: Alkuraya et al., Human Mutations in *NDE1* Cause Extreme Microcephaly with Lissencephaly, The American Journal of Human Genetics (2011), doi:10.1016/j.ajhg.2011.04.003

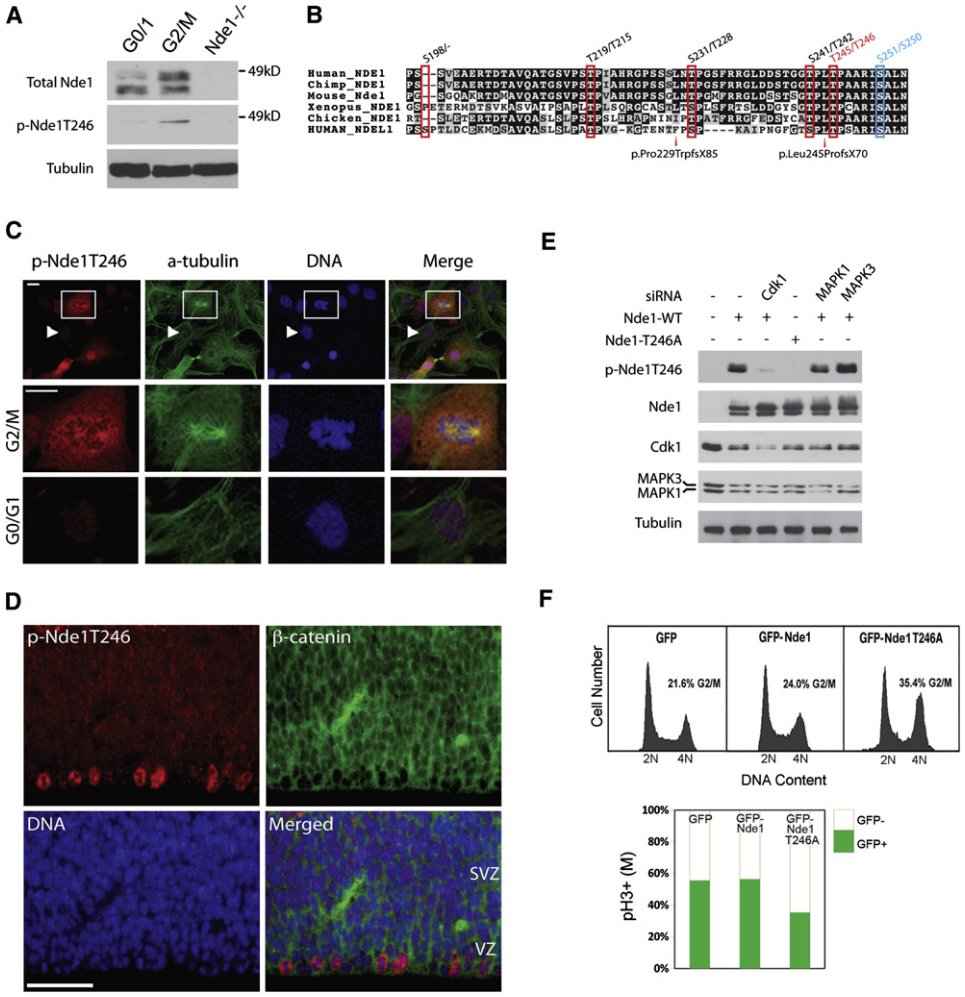

Figure 4. T246 of Nde1 is Phosphorylated by Cdk1 and Is Involved in the G2/M Transition

(A) Nde1 is phosphorylated during mitosis. Immunoblotting of Nde1 with total and phospho-specific Nde1 antibody from serum-starved G0 and mitotically arrested (G2/M) 293T cells and *Nde1*$^{-/-}$ cells (lanes 1, 2, and 3, respectively). A band of slowly migrating phosphorylated Nde1 (p-Nde1) is significantly elevated in the G2/M cell population (lane 2) and absent in the *Nde1*$^{-/-}$-negative control (lane 3), indicating the phospho-Nde1 antibody specificity.

(B) Four out of five putative phosphorylation sites previously identified in Ndel1 are conserved in Nde1(T215, T228, T242, and T246). Among them, T246 and its flanking sequence are the most conserved and represent the only site disrupted in both mutant alleles. Both mutations also disrupt a potential AurA phosphorylation site (S250), on the basis of its sequence homology to Ndel1.

(C) Phospho-specific antibody against Nde1 T246 exclusively recognizes G2- and M-phase MEFs (upper panel). (Lower panels) Representative images of a mitotic cell (marked in square) and an interphase cell (marked by arrowhead). The scale bar indicates 10 μm.

(D) Immunohistological staining of the cerebral cortical ventricular zone from an E14.5 mouse brain with p-Nde1T246 antibody (red) and β-catenin (green) shows preferential staining of M-phase cell along the ventricular surface. The scale bar indicates 50 μm. The ventricular zone (VZ) and subventricular zone (SVZ) are indicated at their corresponding position in the image.

(E) Nde1 was phosphorylated at T246 by Cdk1 but not by MAPK1 or MAPK3. Two nanomoles of *Silencer* Select Pre-Designed and Validated siRNA to Cdk1, MAPK1, and MAPK3 siRNA (Ambion/Applied Biosystems) was cotransfected with 1 μg Nde1-WT/T246A plasmid into 293T cells. Immunosignals were abolished specifically by Cdk1 siRNA or by the Nde1-T246A point mutation but not by siRNA against MAPK1 or MAPK3.

(F) Cell-cycle profiles of 293T cells transfected with GFP, GFP-Nde1, and GFP-Nde1-T246A. An increased 4N (G2/M) population was observed by GFP-Nde1-T246A overexpression, suggesting the important role of p-Nde1T246 in cell-cycle progression. In addition, flow cytometry on the 4N population by phospho-histone H3 (pH3, mitotic marker) reveals that there are a decreased number of mitotic cells in the GFP-Nde1-T246A transfected cells despite the more abundant 4N population, suggesting that a large number of these cells arrested in the G2 phase. The y axis represents the ratio of pH3(+) to pH3(−) cells.

with its role as a target of Cdk1. These data indicate that Nde1 T246 is an essential substrate for Cdk1 and provide a mechanistic explanation for how the removal of the C terminus of Nde1, or loss of the entire Nde1 protein, blocks cell-cycle progression, which would account for the extreme microcephaly caused by *NDE1* mutations.

Loss of *NDE1* or *Nde1* Disrupts Mitotic Progression in Both Human and Mice

Mouse embryonic fibroblasts with *Nde1* mutations (Figures 5A–5D) showed defects in mitotic progression, as evidenced by an increased mitotic index; abnormal spindle structures such as multipolar spindles (Figure 5B); and chromosome

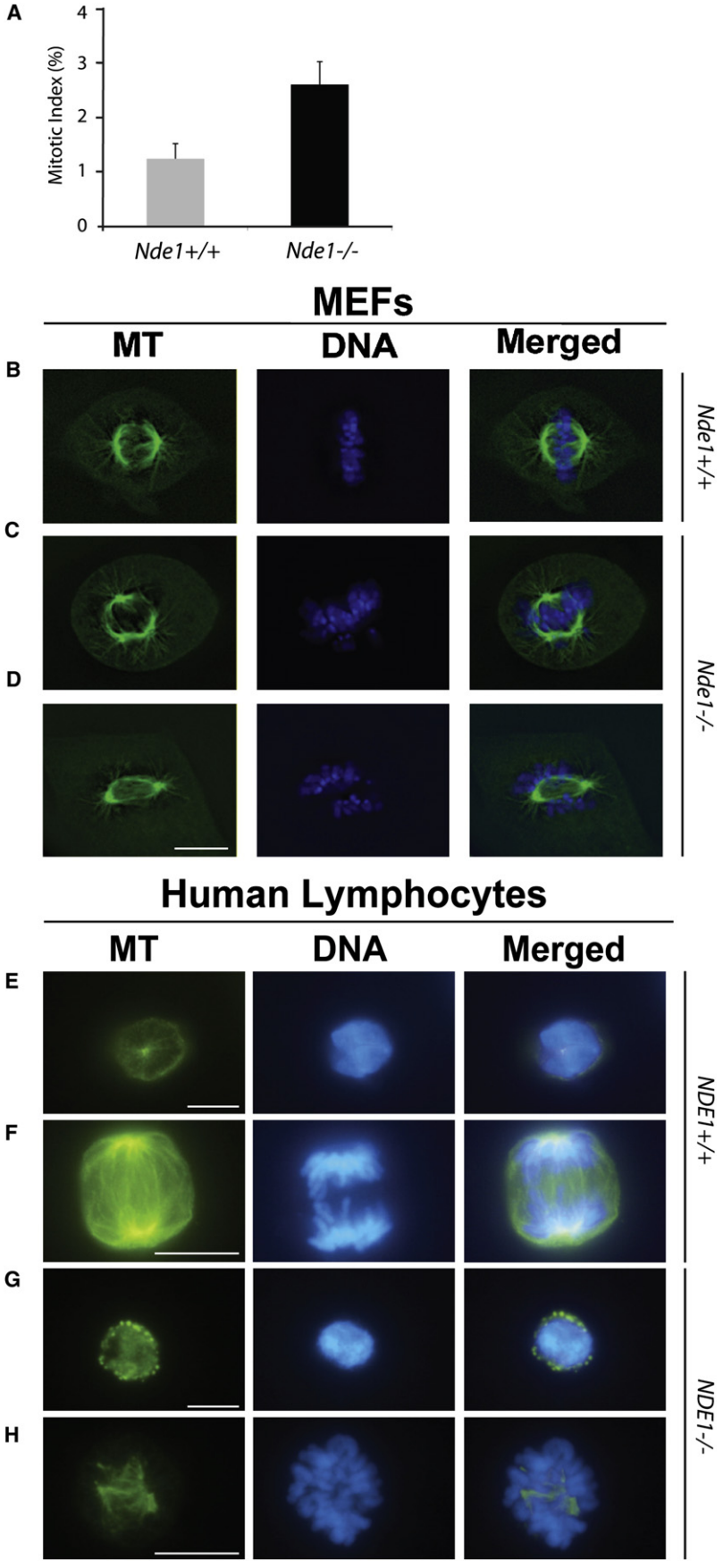

Figure 5. NDE1 Deficiency Leads to Increased Mitotic Index and Abnormal Mitotic Spindles

(A–D) Early-passage (P0-3) primary MEFs derived from wild-type ($Nde1^{+/+}$) and mutant ($Nde1^{-/-}$) embryos were analyzed. (A) Mitotic index increased by approximately 50% in $Nde1^{-/-}$ MEFs compared to that in $Nde1^{+/+}$ MEFs at passage 1 (p value < 0.01, chi-square test of homogeneity for two independent samples; error bar represents standard error of the mean). (B–D) Primary MEFs derived from wild-type ($Nde1^{+/+}$) and mutant ($Nde1^{-/-}$) embryos were analyzed directly for the structure of mitotic spindles by staining with monoclonal antibody for tubulin (in green) and Hoechst for chromosomal DNA (in blue). (B) A normal $Nde1^{+/+}$ M-phase cell. (C) An abnormal $Nde1^{-/-}$ M phase cell with tripolar mitotic spindle and misaligned mitotic chromosomes and (D) an abnormal $Nde1^{-/-}$ mitotic cell with discordant mitotic spindle and chromosome alignments. The scale bar indicates 10 μm. (E–H) *NDE1* patient lymphoblasts exhibit similar defects in mitotic spindle organization. (E and F) Control lymphoblasts showed normal looking nuclei and normal α-tubulin staining. (E) An example of a normal $NDE1^{+/+}$ interphase cell. (F) An example of a normal $NDE1^{+/+}$ M phase cell. (G and H) Patient lymphoblasts showed condensed/fragmentized nuclei and disorganized α-tubulin. (G) An example of an abnormal $NDE1^{-/-}$ interphase cell with nuclear fragmentation and (H) an example of an abnormal $NDE1^{-/-}$ M phase cell with multipolar and disorganized spindles. The scale bar indicates 10 μm. The percentage of mitotic cells found with abnormal spindles was 7% in patient lymphoblasts and compared to 0% in control lymphoblasts ($p < 0.02$, two-tailed chi-square test).

misalignment (Figure 5C). Similarly, patient-derived lymphoblast cells (Figures 5E–5H) also show spindle-structure defects, including tripolar spindles, misaligned mitotic chromosomes, nuclear fragmentation, and abnormal microtubule organizations, further supporting the idea that NDE1 is essential for normal mitotic spindle function. Patient lymphoblasts also showed excessive cell death (data not shown), which could also contribute to the developmental defects. We previously reported that the N-terminal self-association domain of Nde1 is required for proper mitotic spindle assembly and mitotic progression, which presumably accounts for the mitotic defects in *NDE1*- and *Nde1*-null cells.[14] The interesting contrast between the G2 arrest induced by Nde1-T246A overexpression and the M phase arrest resulting from Nde1 depletion presumably reflects the pleiotropic roles of Nde1 in cell-cycle regulation and is discussed in greater detail below.

Discussion

Our data indicate that loss of *NDE1* produces profound defects in cerebral cortical size and organization as well as less profound defects in somatic size. Both of the identified *NDE1* mutations truncate the C terminus of the NDE1 protein, preventing normal dynein binding. Whereas the overexpressed proteins are somewhat unstable, they retain LIS1-binding activity and so in principle could act as dominant-negative proteins. However, the absence of a genetically dominant phenotype, the absence of detectable mutant proteins in patient cells, and the similarity of the phenotype in the three patients described here (as well as additional patients and an additional mutant allele described by Bakircioglu et al.[19]), all argue strongly that the mutations act as simple null alleles.

The C terminus of NDE1 is also mutated by the recurrent 16p inversions that are associated with acute myelogenous leukemia (AML), which disrupts exon 8 of *NDE1*, encoding the extreme C terminus of the protein.[34] Existing pedigree analysis and medical follow-up of families 1 and 2, although somewhat limited, has so far not suggested the presence of AML or other leukemia in homozygous or heterozygous carriers of *NDE1* mutations, though more extensive analysis of additional families is needed. On the other hand, our biochemical analysis suggests that the AML disruptions, if they create a stable truncated protein, could potentially create abnormal proteins with preserved LIS1 binding but abnormal dynein binding, which might contribute to leukemogenesis.

Whereas mice lacking Nde1 show about a one-third reduction in brain mass,[14] neuronal migration is only moderately deficient, but human NDE1 mutations cause a decrease of more than 50% in cortical volume and striking architectural disturbances that suggest severely abnormal neuronal migration (see also Bakircioglu et al.[19]). The more striking brain defects seen in humans harboring *NDE1* mutations, especially the marked architectural defects, could reflect morphological or quantitative defects in the radial glial cells that normally act as guides for migrating neurons, or they could reflect the larger human brain and its increased opportunities for defects in neurogenesis. Alternatively, the differences could reflect a greater role for *NDE1* in migrating neurons in humans than in mice, in parallel to the much more profound defects in neuronal migration in humans than in mice after removal of one allele of LIS1. The Nde1 paralog, Ndel1, is highly similar structurally to Nde1, more highly expressed in postmitotic neurons, and appears to have larger roles in cell proliferation outside the brain, mitotic spindle orientation, and neuronal migration.[16,27,29,33,35–38] The details of potential genetic redundancy between NDE1 and NDEL1 could also contribute to the differences between mice and humans. The overlapping functions of NDE1 and NDEL1 could also relate to distinct cellular phenotypes, namely interference with normal phosphorylation of NDE1, which arrests cells in G2 phase, versus simple loss of NDE1, which arrests cells in M phase. Perhaps redundant functions of NDEL1 allow NDE1-deficient cells to traverse G2, whereas lack of normal NDE1 phosphorylation might induce abnormal protein complexes that interfere with both NDE1 and NDEL1 function, preventing transit through mitosis.

Humans with *NDE1* mutations show modestly reduced height and weight as well as cerebral cortical size, though the defect in head circumference (typically 10 to 14 SD below the mean) was more marked statistically than defects in height and weight (typically 2 to 5 SD below mean). The decreased body size could reflect roles of NDE1 in other tissues, although more specific hypothalamic defects or nutritional explanations related to the patients' poor neurological function cannot be ruled out. Mice with *Nde1* mutations show at most a slight, statistically insignificant reduction in body mass.[14] Because *NDE1*, like many other microcephaly genes, is expressed in many developing tissues,[13] the more severe involvement of the brain is generally regarded as reflecting its more limited ability to regulate its size, given that most brain cells are postmitotic, but other mechanisms might also contribute to this tissue specificity.

Finally, although analysis of archived DNA samples from the original microlissencephaly family studied by Norman and Roberts[11] did not reveal a detectable mutation in *NDE1* (data not shown), the similarity of the *NDE1* phenotype to the Norman Roberts syndrome is striking, and some other cases of microlissencephaly also do not show *NDE1* mutations. Hence, this classical form of microlissencephaly might ultimately reflect defects in proteins that function in close concert with NDE1 in this highly conserved centrosomal pathway.

Supplemental Data

Supplemental Data include one figure, two tables, and six movies and can be found with this article online at http://www.cell.com/AJHG/.

Acknowledgments

We are grateful to the families, clinicians, and researchers who contributed to this study, including reviews of the MRI findings by Bernard Chang and Annapurna Poduri. We thank members of the Microcephaly Collaborative (Table S2) for contributing patient samples not directly used in this study. F.S.A., G.H.M, and C.A.W. are supported by a Collaborative Research Grant from the Dubai-Harvard Foundation for Medical Research. F.S.A. is also supported by the King Abdulaziz City for Science and Technology (Grant 10-MED941-20/Saudi Arabia). X.C. is supported by the National Institute of General Medical Sciences (T32 GM007726-35). G.H.M. was supported by National Alliance for Research on Schizophrenia and Depression as a Lieber Young Investigator. Y.F. is supported by the NICHD (R01HD56380), and the Schweppe Foundation. C.A.W is supported by the NINDS (RO1 NS 32457) the Fogarty International Center (R21 NS061772), the Manton Center for Orphan Disease Research, the National Library of Medicine Family Foundation, and the Simons Foundation. Genotyping at the Center for Inherited Disease Research is funded through a federal contract from the National Institutes of Health (NIH) to The Johns Hopkins University (HHSN268200782096C and NIH N01-HG-65403). Genotyping at Children's Hospital Boston is supported by the Intellectual and Developmental Disabilities Research Centers (P30 HD18655). SNP genotyping of family 2 was performed through the NIH Neuroscience Microarray Consortium. Genotyping at the Broad Institute is supported by the National Human Genome Research Institute. C.A.W. is an Investigator of the Howard Hughes Medical Institute.

Received: January 22, 2011
Revised: March 25, 2011
Accepted: April 7, 2011
Published online: April 28, 2011

Web Resources

The URLs for data presented herein are as follows:

1000 Genomes Project, http://www.1000genomes.org/
GenBank, http://www.ncbi.nlm.nih.gov/Genbank/
HGVS Guidelines, http://www.hgvs.org/rec.html
Online Mendelian Inheritance in Man (OMIM), http://www.omim.org
Scansite, http://scansite.mit.edu
UCSC Genome Browser, http://genome.ucsc.edu/cgi-bin/hgGateway

References

1. Thornton, G.K., and Woods, C.G. (2009). Primary microcephaly: Do all roads lead to Rome? Trends Genet. *25*, 501–510.
2. Wynshaw-Boris, A., Pramparo, T., Youn, Y.H., and Hirotsune, S. (2010). Lissencephaly: Mechanistic insights from animal models and potential therapeutic strategies. Semin. Cell Dev. Biol. *21*, 823–830.
3. Dobyns, W.B., Reiner, O., Carrozzo, R., and Ledbetter, D.H. (1993). Lissencephaly. A human brain malformation associated with deletion of the LIS1 gene located at chromosome 17p13. JAMA *270*, 2838–2842.
4. Gleeson, J.G., Allen, K.M., Fox, J.W., Lamperti, E.D., Berkovic, S., Scheffer, I., Cooper, E.C., Dobyns, W.B., Minnerath, S.R., Ross, M.E., and Walsh, C.A. (1998). Doublecortin, a brain-specific gene mutated in human X-linked lissencephaly and double cortex syndrome, encodes a putative signaling protein. Cell *92*, 63–72.
5. Hong, S.E., Shugart, Y.Y., Huang, D.T., Shahwan, S.A., Grant, P.E., Hourihane, J.O., Martin, N.D., and Walsh, C.A. (2000). Autosomal recessive lissencephaly with cerebellar hypoplasia is associated with human RELN mutations. Nat. Genet. *26*, 93–96.
6. Poirier, K., Keays, D.A., Francis, F., Saillour, Y., Bahi, N., Manouvrier, S., Fallet-Bianco, C., Pasquier, L., Toutain, A., Tuy, F.P., et al. (2007). Large spectrum of lissencephaly and pachygyria phenotypes resulting from de novo missense mutations in tubulin alpha 1A (TUBA1A). Hum. Mutat. *28*, 1055–1064.
7. Bilgüvar, K., Oztürk, A.K., Louvi, A., Kwan, K.Y., Choi, M., Tatli, B., Yalnizoğlu, D., Tüysüz, B., Cağlayan, A.O., Gökben, S., et al. (2010). Whole-exome sequencing identifies recessive WDR62 mutations in severe brain malformations. Nature *467*, 207–210.
8. Nicholas, A.K., Khurshid, M., Désir, J., Carvalho, O.P., Cox, J.J., Thornton, G., Kausar, R., Ansar, M., Ahmad, W., Verloes, A., et al. (2010). WDR62 is associated with the spindle pole and is mutated in human microcephaly. Nat. Genet. *42*, 1010–1014.
9. Yu, T.W., Mochida, G.H., Tischfield, D.J., Sgaier, S.K., Flores-Sarnat, L., Sergi, C.M., Topçu, M., McDonald, M.T., Barry, B.J., Felie, J.M., et al. (2010). Mutations in WDR62, encoding a centrosome-associated protein, cause microcephaly with simplified gyri and abnormal cortical architecture. Nat. Genet. *42*, 1015–1020.
10. Dobyns, W.B., Stratton, R.F., and Greenberg, F. (1984). Syndromes with lissencephaly. I: Miller-Dieker and Norman-Roberts syndromes and isolated lissencephaly. Am. J. Med. Genet. *18*, 509–526.
11. Norman, M.G., Roberts, M., Sirois, J., and Tremblay, L.J. (1976). Lissencephaly. Can. J. Neurol. Sci. *3*, 39–46.
12. Efimov, V.P., and Morris, N.R. (2000). The LIS1-related NUDF protein of Aspergillus nidulans interacts with the coiled-coil domain of the NUDE/RO11 protein. J. Cell Biol. *150*, 681–688.
13. Feng, Y., Olson, E.C., Stukenberg, P.T., Flanagan, L.A., Kirschner, M.W., and Walsh, C.A. (2000). LIS1 regulates CNS lamination by interacting with mNudE, a central component of the centrosome. Neuron *28*, 665–679.
14. Feng, Y., and Walsh, C.A. (2004). Mitotic spindle regulation by Nde1 controls cerebral cortical size. Neuron *44*, 279–293.
15. McKenney, R.J., Vershinin, M., Kunwar, A., Vallee, R.B., and Gross, S.P. (2010). LIS1 and NudE induce a persistent dynein force-producing state. Cell *141*, 304–314.
16. Wynshaw-Boris, A. (2007). Lissencephaly and LIS1: Insights into the molecular mechanisms of neuronal migration and development. Clin. Genet. *72*, 296–304.
17. Pawlisz, A.S., Mutch, C., Wynshaw-Boris, A., Chenn, A., Walsh, C.A., and Feng, Y. (2008). Lis1-Nde1-dependent neuronal fate control determines cerebral cortical size and lamination. Hum. Mol. Genet. *17*, 2441–2455.
18. Yingling, J., Youn, Y.H., Darling, D., Toyo-Oka, K., Pramparo, T., Hirotsune, S., and Wynshaw-Boris, A. (2008). Neuroepithelial stem cell proliferation requires LIS1 for precise spindle orientation and symmetric division. Cell *132*, 474–486.
19. Bakircioglu, M., Carvalho, O.P., Khurshid, M., Cox, J.J., Tuysuz, B., Barak, T., Yilmaz, S., Caglayan, A.O., Dincer, A., Nicholas, A.K., et al. (2011). The essential role of centrosomal NDE1 in human cerebral cortex neurogenesis. Am. J. Hum. Genet. *88*, this issue, ■■■–■■■.

20. Vergnolle, M.A., and Taylor, S.S. (2007). Cenp-F links kinetochores to Ndel1/Nde1/Lis1/dynein microtubule motor complexes. Curr. Biol. *17*, 1173–1179.
21. Sasaki, S., Shionoya, A., Ishida, M., Gambello, M.J., Yingling, J., Wynshaw-Boris, A., and Hirotsune, S. (2000). A LIS1/NUDEL/cytoplasmic dynein heavy chain complex in the developing and adult nervous system. Neuron *28*, 681–696.
22. Stehman, S.A., Chen, Y., McKenney, R.J., and Vallee, R.B. (2007). NudE and NudEL are required for mitotic progression and are involved in dynein recruitment to kinetochores. J. Cell Biol. *178*, 583–594.
23. Hirohashi, Y., Wang, Q., Liu, Q., Li, B., Du, X., Zhang, H., Furuuchi, K., Masuda, K., Sato, N., and Greene, M.I. (2006). Centrosomal proteins Nde1 and Su48 form a complex regulated by phosphorylation. Oncogene *25*, 6048–6055.
24. Bond, J., Roberts, E., Mochida, G.H., Hampshire, D.J., Scott, S., Askham, J.M., Springell, K., Mahadevan, M., Crow, Y.J., Markham, A.F., et al. (2002). ASPM is a major determinant of cerebral cortical size. Nat. Genet. *32*, 316–320.
25. Bond, J., Roberts, E., Springell, K., Lizarraga, S.B., Scott, S., Higgins, J., Hampshire, D.J., Morrison, E.E., Leal, G.F., Silva, E.O., et al. (2005). A centrosomal mechanism involving CDK5RAP2 and CENPJ controls brain size. Nat. Genet. *37*, 353–355.
26. Desir, J., Cassart, M., David, P., Van Bogaert, P., and Abramowicz, M. (2008). Primary microcephaly with ASPM mutation shows simplified cortical gyration with antero-posterior gradient pre- and post-natally. Am. J. Med. Genet. A. *146A*, 1439–1443.
27. Derewenda, U., Tarricone, C., Choi, W.C., Cooper, D.R., Lukasik, S., Perrina, F., Tripathy, A., Kim, M.H., Cafiso, D.S., Musacchio, A., and Derewenda, Z.S. (2007). The structure of the coiled-coil domain of Ndel1 and the basis of its interaction with Lis1, the causal protein of Miller-Dieker lissencephaly. Structure *15*, 1467–1481.
28. Dephoure, N., Zhou, C., Villén, J., Beausoleil, S.A., Bakalarski, C.E., Elledge, S.J., and Gygi, S.P. (2008). A quantitative atlas of mitotic phosphorylation. Proc. Natl. Acad. Sci. USA *105*, 10762–10767.
29. Mori, D., Yano, Y., Toyo-oka, K., Yoshida, N., Yamada, M., Muramatsu, M., Zhang, D., Saya, H., Toyoshima, Y.Y., Kinoshita, K., et al. (2007). NDEL1 phosphorylation by Aurora-A kinase is essential for centrosomal maturation, separation, and TACC3 recruitment. Mol. Cell. Biol. *27*, 352–367.
30. Yan, X., Li, F., Liang, Y., Shen, Y., Zhao, X., Huang, Q., and Zhu, X. (2003). Human Nudel and NudE as regulators of cytoplasmic dynein in poleward protein transport along the mitotic spindle. Mol. Cell. Biol. *23*, 1239–1250.
31. Yaffe, M.B., Leparc, G.G., Lai, J., Obata, T., Volinia, S., and Cantley, L.C. (2001). A motif-based profile scanning approach for genome-wide prediction of signaling pathways. Nat. Biotechnol. *19*, 348–353.
32. Niethammer, M., Smith, D.S., Ayala, R., Peng, J., Ko, J., Lee, M.S., Morabito, M., and Tsai, L.H. (2000). NUDEL is a novel Cdk5 substrate that associates with LIS1 and cytoplasmic dynein. Neuron *28*, 697–711.
33. Shu, T., Ayala, R., Nguyen, M.D., Xie, Z., Gleeson, J.G., and Tsai, L.H. (2004). Ndel1 operates in a common pathway with LIS1 and cytoplasmic dynein to regulate cortical neuronal positioning. Neuron *44*, 263–277.
34. Van der Reijden, B.A., Massop, M., Simons, A., de Witte, T., Breuning, M., and Jansen, J.H. (2010). The NDE1 gene is disrupted by the inv(16) in 90% of cases with CBFB-MYH11-positive acute myeloid leukemia. Leukemia *24*, 857–859.
35. Lam, C., Vergnolle, M.A., Thorpe, L., Woodman, P.G., and Allan, V.J. (2010). Functional interplay between LIS1, NDE1 and NDEL1 in dynein-dependent organelle positioning. J. Cell Sci. *123*, 202–212.
36. Sasaki, S., Mori, D., Toyo-oka, K., Chen, A., Garrett-Beal, L., Muramatsu, M., Miyagawa, S., Hiraiwa, N., Yoshiki, A., Wynshaw-Boris, A., and Hirotsune, S. (2005). Complete loss of Ndel1 results in neuronal migration defects and early embryonic lethality. Mol. Cell. Biol. *25*, 7812–7827.
37. Toyo-Oka, K., Sasaki, S., Yano, Y., Mori, D., Kobayashi, T., Toyoshima, Y.Y., Tokuoka, S.M., Ishii, S., Shimizu, T., Muramatsu, M., et al. (2005). Recruitment of katanin p60 by phosphorylated NDEL1, an LIS1 interacting protein, is essential for mitotic cell division and neuronal migration. Hum. Mol. Genet. *14*, 3113–3128.
38. Yamada, M., Toba, S., Yoshida, Y., Haratani, K., Mori, D., Yano, Y., Mimori-Kiyosue, Y., Nakamura, T., Itoh, K., Fushiki, S., et al. (2008). LIS1 and NDEL1 coordinate the plus-end-directed transport of cytoplasmic dynein. EMBO J. *27*, 2471–2483.